Journal of Artificial Intelligence and Data Mining (JAIDM), Vol. 14, No. 3, 2026, 433-452.

Shahrood University of Technology

Journal of Artificial Intelligence and Data Mining (JAIDM)
Journal homepage: http://jad.shahroodut.ac.ir

Research paper

Beyond Raw Time-Series Indices: Robust Rice Mapping with Phenological-informed LSTM Framework Using Multi-Sensor Satellite Data

Fateme Namazi[1], Mehdi Ezoji[1]* and Ebadat Ghanbari Parmehr[2]

1. Faculty of Electrical and Computer Engineering, Babol Noshirvani University of Technology, Babol, Iran.
2. Department of Geomatics, Faculty of Civil Engineering, Babol Noshirvani University of Technology, Babol, Iran.

Article Info

Article History:
Received 28 April 2026
Revised 29 June 2026
Accepted 01 August 2026

DOI:10.22044/jadm.2026.17643.2920

Keywords:
Rice Crop Mapping, Phenology, Sentinel-1/2, Correlation Analysis, LSTM.

**Corresponding author: m.ezoji@nit.ac.ir (M. Ezoji).*

Abstract

Accurate rice mapping is crucial for food security, water management, and long-term agricultural planning. This study proposes a phenology-informed LSTM framework that integrates multi-source Sentinel-1 and Sentinel-2 time-series data for robust rice mapping. Sentinel-2 optical images and Sentinel-1 SAR images were preprocessed using cloud-pixel removal, 10-day temporal compositing, and interpolation of missing observations to generate complete and temporally consistent 18-step time series over a 180-day observation period. Three indices, including Sentinel-2-derived NDVI and LSWI and Sentinel-1-derived CR, were extracted to represent vegetation greenness, surface/vegetation moisture, and radar backscatter dynamics. To incorporate rice phenological prior knowledge, reference rice phenology curves were constructed for these indices, and a sliding-window correlation analysis was applied between each pixel-level index trajectory and the corresponding reference curve. This process generated three correlation-based temporal similarity sequences, C_NDVI, C_LSWI, and C_CR, which describe how closely each pixel follows the characteristic rice growth pattern. The raw indices, correlation-based features, and their combined representation were then evaluated as sequential inputs to an LSTM classifier. The results showed that the correlation-based feature set achieved the best performance, with an overall accuracy of 99.81%, an error rate of 0.19%, and an F1-score of 0.9950. Compared with raw time-series indices and the combined feature set, the correlation-based representation improved the discrimination of rice paddies from spectrally similar classes such as water bodies and weeds. The results demonstrate that integrating phenology-informed correlation features with LSTM-based temporal learning provides an effective framework for accurate rice mapping in fragmented and cloud-prone agricultural landscapes.

1. Introduction

In recent years, global food security has emerged as a central concern within the international policy agenda, as evidenced by the United Nations Sustainable Development Goals. Nevertheless, rapid population growth and regional conflicts persistently threaten the stability of global food production [1]. Among staple crops, rice is particularly vital, feeding more than half of the world's population and occupying more than 12% of arable land [2, 3]. Accurate rice mapping is therefore crucial for food security, water management, climate change mitigation, and sustainable land use [4]. Traditional field surveys are expensive and limited, especially in smallholder systems, whereas remote sensing offers a scalable, cost-effective solution for agricultural monitoring [5]. Sentinel-2 and Sentinel-1 have emerged as valuable resources for rice mapping [6–8]. Optical indices (NDVI, EVI, LSWI) capture phenological changes [9, 10]. However, frequent cloud cover and persistent rainfall in tropical and subtropical areas often restrict the use of optical sensors [8]. In contrast, Synthetic Aperture Radar (SAR), with its all-weather, cloud-penetrating capability and sensitivity to surface water and structural features, provides complementary information [11]. Their combined use significantly improves the accuracy and reliability of rice mapping [12–16].

Rice mapping approaches are broadly categorized into spectral learning and phenology-based methods. Spectral learning techniques, which applies classifiers such as SVM [9], RF[17], and DT [12, 18] directly to spectral bands or indices, often limited by their inability to capture complex temporal dynamics. While deep learning models – including Convolutional Neural Networks (CNN)[19], Long Short-Term Memory (LSTM) networks [10, 20], and Convolutional LSTM (ConvLSTM) models [21, 22]- address this by capturing spatiotemporal patterns, they present other challenges. These models demand large training datasets and are highly sensitive to the quality and resolution of remote sensing issues such as noise, missing observations, or low spatial resolution can severely degrade their mapping accuracy.

Phenology-based approaches utilize phenological parameters such as Start of Season (SOS), End of Season (EOS), Peak of Season (POS), and Length of Season (LOS). Classification is performed using threshold-based [6, 9, 23, 24], statistical, or machine learning techniques such as SVM, RF, or DT [7, 25, 26]. A primary drawback of these methods is that the accurate calculation of phenological characteristics depends on index values at specific time points, which may be influenced by abnormal fluctuations. Such anomalies can result from poor image quality due to cloud contamination [27], spectral confusion with weeds under certain conditions [23], human activities, or variations in cropping calendars (for example, early or late planting in regions with multiple cropping cycles). Conventional classifiers also lack recurrent structures, which restricts their ability to capture temporal dependencies in crop phenology.

To address these challenges, our previous research introduced correlation-based features that measure pixel-level similarity to a reference phenology [28]. These features enhance discriminative power while filtering noise by suppressing spurious temporal changes. The robustness of the correlation-based features makes them particularly suitable as inputs for recurrent neural networks (RNNs) like LSTMs, whose memory gates reduce vanishing gradients and effectively capture long-term dependencies.

The present study builds upon our previous phenology-based rice-mapping investigations [28, 29], but differs from them in both feature representation and classification strategy. In [28], phenological similarity was measured using correlations between Sentinel-2-derived NDVI and LSWI time series and reference rice phenology curves. The approach was subsequently extended in [29] by incorporating Sentinel-1-derived CR data alongside NDVI and LSWI. In those studies, the correlation curves were mainly summarized using manually selected descriptors, including the maximum correlation value and its temporal position, with the final classification performed using conventional decision rules or an SVM-RBF classifier. In contrast, the present framework preserves the complete temporal correlation sequences rather than reducing them to a small number of scalar descriptors. For each pixel, three 18-step correlation sequences, C_NDVI, C_LSWI, and C_CR, are generated and directly supplied to an LSTM network. Consequently, the classifier can learn temporal dependencies and nonlinear relationships across the entire observation period, including temporal shifts associated with early or late cultivation. The integrated method, combining spectral and correlation-based features, yields highly accurate rice cultivation maps. The framework was implemented in Google Colab and the GEE API.

2. Study Area and Datasets

2.1. Study Area

Mazandaran Province, located between the Alborz Mountains and the Caspian Sea (Figure 1), has a temperate and humid climate that supports its status as a key agricultural region by several characteristics: (i) widespread rice cultivation occurs in small, inundated paddy fields (generally < 0.5 hectares), which are highly fragmented and interspersed with settlements and other crops; (ii) a diverse array of crops is grown, including various rice cultivars, citrus, deciduous trees, wheat, and vegetables, creating a complex cropping pattern; (iii) close spatial proximity of rice paddies to plots dedicated to other crop types; and (iv) the region's frequent cloud cover, which often obstructs satellite observations, complicates the acquisition of high-quality satellite imagery. Furthermore, a wide range of rice cultivars is grown in the province. In some fields, a multi-cropping system is practiced, introducing variability in planting and harvesting schedules across the landscape.

In the studied region, rice cultivation is primarily categorized into low-yielding and high-yielding types with similar planting periods but differing growth durations; high-yielding varieties are distinguished by longer growth durations and greater productivity. The total growth cycle of rice ranges from 80 to 120 days, depending on the specific cultivar, with paddy fields typically remaining flooded for approximately 60 to 90 days after sowing. The spatial configuration of horticultural crops is highly fragmented and dispersed, resulting in a complex and irregular cropping pattern. In recent years, favorable climatic conditions have significantly contributed to the expansion of double-season rice cultivation in the region. These factors—namely cloud cover, small field sizes, fine-grained fragmentation, mixed land use, and variable crop calendars—make Mazandaran a demanding and representative case study for rice mapping.

2.2. Datasets

This study uses satellite data from the Sentinel-1 and Sentinel-2 missions to monitor rice cultivation dynamics in Mazandaran Province during the growing season (April to October). Both missions are part of the Copernicus Earth observation program and include twin polar-orbiting satellites. Sentinel-1 has a C-band Synthetic Aperture Radar (SAR) sensor that operates independently of daylight and weather conditions. It collects data at a spatial resolution of 10 meters with a revisit frequency of six days at the equator. For this study, Sentinel-1 Ground Range Detected (GRD) products were employed in Interferometric Wide (IW) swath mode, with both VV (vertical transmit/vertical receive) and VH (vertical transmit/horizontal receive) polarizations. The VH channel, in particular, is known for its higher sensitivity to water and flood situations, which is important for detecting inundated rice fields [9].

Complementarily, Sentinel-2 imagery was employed to derive multispectral vegetation and moisture indices. The Sentinel-2 Multispectral Instrument (MSI) captures 13 spectral bands in the visible, near-infrared (NIR), and shortwave infrared (SWIR) ranges, with spatial resolutions of 10, 20, or 60 meters depending on the band [30]. The Level-2A surface reflectance product, which had been preprocessed for atmospheric correction and orthorectification, was used in this study. Cloud-contaminated pixels were eliminated using the quality assessment (QA) band, and 10-day mean composites were generated to reduce noise and improve temporal consistency. Vegetation and moisture indices were subsequently calculated to characterize crop growth stages. All Sentinel data were accessible through the Google Earth Engine (GEE) platform, which facilitated data filtering, masking, and temporal compositing.

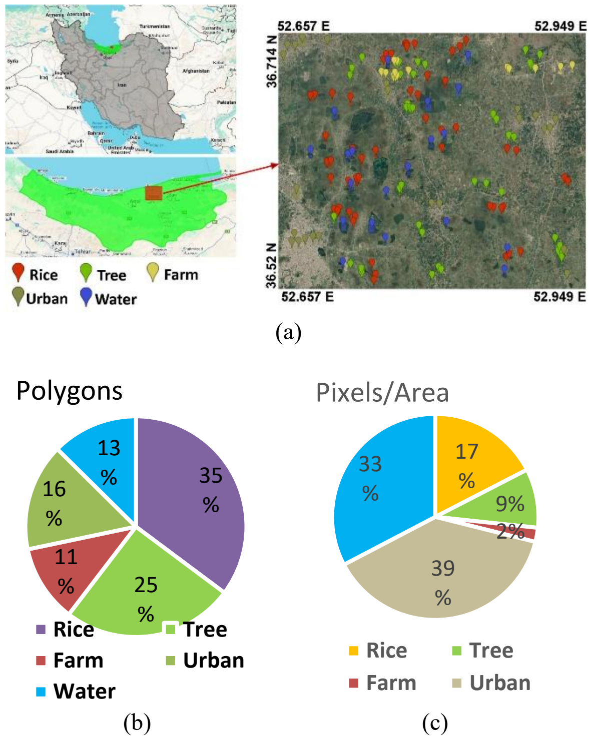

Figure 1. (a) Field survey locations. Frequency chart of labels in terms of (b) polygons (c) pixels.

2.3. Field Data and Dataset Labelling

The study area is located in Mazandaran Province, northern Iran, between latitudes 36.52°N and 36.71°N and longitudes 52.65°E and 52.95°E (Figure 1). Ground-truth data were collected from March to August during the 2021–2023 rice-growing seasons using two complementary approaches. First, field surveys were conducted using GPS/mobile devices to record representative rice and non-rice areas. Second, additional labeled polygons were collected through visual interpretation of high-resolution satellite imagery and the Google Earth Engine (GEE) platform. The collected polygons were assigned to five land-cover classes: rice, tree/orchard, urban, water, and farm. The farm class included non-rice agricultural fields, while tree/orchard represented horticultural areas such as citrus orchards.

After labeling, pixel-level samples were extracted from the labeled polygons. To reduce spatial leakage between training and testing data, the dataset was divided at the polygon level rather than at the pixel level. The complete dataset contained 159 labeled polygons and 65,507 extracted samples. The polygons were divided into a model-development set containing 50 polygons and an independent test set containing 109 polygons. The model-development set included 16,269 samples, whereas the independent test set contained 49,238 samples. The model-development samples were further divided into final training and validation subsets using an 80:20 random split, resulting in 13,015 training samples and 3,254 validation samples. Table 1 reports the class-wise distribution of polygons and samples.

Table 1. Class-wise distribution of polygons and samples.

	Polygons			Samples			Development Samples	
Class	**Total polygons**	**Model-development polygons**	**Independent-test polygons**	**Total samples**	**Model-development samples**	**Independent-test samples**	**Final training samples**	**Validation samples**
Rice	56	13	43	11972	2701	9271	2178	523
Tree	40	14	26	6590	2223	4367	1772	451
Urban	25	8	17	24459	3514	20945	2786	728
Water	20	6	14	20834	7363	13471	5897	1466
Farm	18	9	9	1652	468	1184	382	86
Total	159	50	109	65507	16269	49238	13015	3254

3. Methodology

The integrated framework for the proposed rice crop mapping is illustrated in Figure 2. This workflow summarizes the complete feature-generation process, including preprocessing, index extraction, reference phenology construction, correlation-based feature generation, and feature-set integration. The detailed architecture of the LSTM classifier used after feature-set construction is further presented. Centered on spectral index time-series analysis and Long Short-Term Memory (LSTM) networks, the proposed methodology consists of five main stages: (1) preprocessing of Sentinel-1 and Sentinel-2 satellite time-series data, (2) selection and extraction of relevant spectral indices, (3) derivation of rice growth phenology curves from the selected indices, (4) feature extraction through correlation analysis, and (5) rice mapping using an LSTM-based model fed by raw time-series indices, correlation-based features, or their combined representation.

3.1. Pre-processing and Extraction of Time Series Indices

Multitemporal datasets acquired from Sentinel-1 (SAR) and Sentinel-2 (optical) platforms were subjected to standard preprocessing procedures to ensure data consistency and reliability. The workflow consisted of four key steps:

1. **Cloudy Pixel Removal:** Sentinel-2 quality flags were used to remove cloudy pixels. This step was essential due to frequent cloud cover in the study area, particularly during the monsoon season, which coincides with rice cultivation.
2. **Ten-Day Quantization:** To align the differing revisit cycles of Sentinel-1 (6-day) and Sentinel-2 (5-day), images were aggregated into 10-day intervals by averaging valid observations. This period optimizes the trade-off between temporal resolution and data quality. Shorter intervals (e.g., 5 days) increase missing data due to cloud cover, while longer intervals (e.g., 20 days) reduce the temporal detail necessary for phenological analysis. The number of valid Sentinel-2 scenes per 10-day interval varied from zero to three; robust interpolation was required to ensure data continuity.
3. **Gap-Filling:** Missing pixel values due to cloud removal or data gaps were filled via interpolation using the method detailed in Table 1. This ensured the generation of a complete, 18-point series spanning the 180-day study period for each pixel.
4. **Index Extraction:** Three indices were calculated for each 10-day interval:
   - **NDVI (Sentinel-2):** Measures vegetation health, capturing the greenness dynamics of rice during vegetative and reproductive stages.
   - **LSWI (Sentinel-2):** Indicates water content in vegetation and soil,

particularly useful for detecting flooding stages in rice paddies.

- **CR (Sentinel-1):** Captures backscatter properties to provide cloud-insensitive observations of canopy structure and water dynamics.

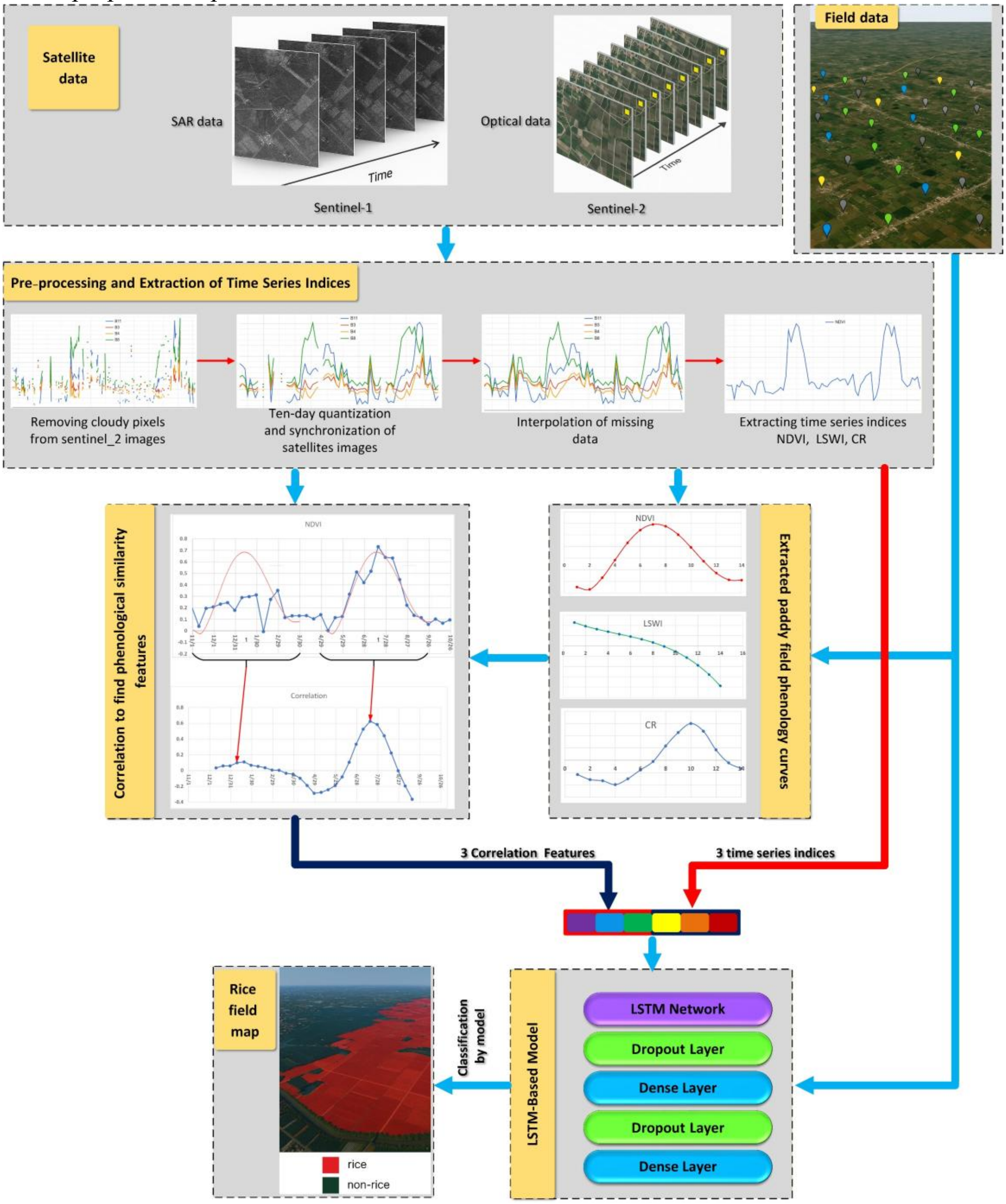

Figure 2. Workflow of the proposed rice mapping framework, including multi-source Sentinel-1/Sentinel-2 preprocessing, extraction of NDVI, LSWI, and CR time-series indices, construction of reference rice phenology curves, sliding-window correlation analysis, generation of correlation-based features, feature-set integration, and LSTM-based rice/non-rice classification.

3.2. Selection the appropriate indices for Sentinel-2 and Sentinel-1

The paddy rice cultivation cycle is broadly categorized into two primary phenological phases: vegetative and reproductive periods. The vegetative phase, which encompasses seedling emergence, transplantation, and tillering, is marked by rapid growth and increasing vegetation coverage. During this stage, the field surface is a heterogeneous mixture of water, rice plants, and soil. The subsequent reproductive phase, including heading and ripening, involves leaf senescence, yellowing, and a decline in vegetation coverage. These distinct temporal phenological characteristics can be effectively detected through time-series analysis of remote sensing imagery, forming the basis of the phenological method to delineate the preliminary distribution of rice paddy areas. Based on a review of relevant indices, the Normalized Difference Vegetation Index (NDVI) and the Land Surface Water Index (LSWI) from Sentinel-2, along with the Cross-Ratio (CR) from Sentinel-1, were selected for this study. NDVI serves as a key indicator of vegetative vigor, biomass accumulation, and canopy greenness. During the rice growth cycle, NDVI follows a dynamic phenological pattern: it begins with low values at the seedling stage, increases rapidly during tillering and elongation stages with biomass accumulation, and peaks at the heading stage. Subsequently, NDVI values decrease during ripening and senescence due to chlorophyll degradation and loss of canopy greenness.

In parallel, LSWI provides complementary information by recording surface water content and vegetation. Its temporal profile is also closely related to rice phenology. High LSWI values in the early stages correspond to flooded field conditions during land preparation and planting. As the rice canopy develops and densifies, surface water becomes less detectable from satellite observations, leading to a gradual decrease in LSWI. This decrease continues until maturity, when fields are drained in preparation for harvest. The NDVI [31] and LSWI [32] are computed using the following equations:

$$NDVI = \frac{NIR - RED}{NIR + RED} \tag{1}$$

$$LSWI = \frac{NIR - SWIR}{NIR + SWIR} \tag{2}$$

where NIR, RED, and SWIR represent the surface reflectance values in the near-infrared, red, and shortwave infrared spectral bands, respectively.

CR is a temporal feature extraction technique increasingly utilized in remote sensing to characterize dynamic changes. In the context of Sentinel-1 SAR data, CR serves as a robust descriptor of phenological transitions for crops like rice, whose growth cycles are associated with distinct biophysical and structural changes detectable by radar backscatter. Crop phenology - the sequence of biological processes during plant development, including emergence, tillering, flowering, and senescence- is typically marked by variations in plant structure and water content. These changes are sensitively detected by dual-polarized SAR signals (VH and VV), especially the VH polarization, which responds strongly to volumetric scattering from the plant canopy and surface moisture. The CR which is highly effective for tracking rice growth is calculated as the ratio of these two polarizations [8]:

$$CR = \frac{VH}{VV} \tag{3}$$

This formulation encodes the relative relationships among the temporal observations, making it invariant to monotonic transformations and certain radiometric inconsistencies. Consequently, CR effectively captures the shape of the phenological curve rather than its absolute amplitude. This property is particularly useful for distinguishing crop types or growth stages with similar spectral/radar signatures but different temporal dynamics.

Key phenological stages in rice cultivation produce distinctive patterns in the VH backscatter time series: transplanting (marked by low backscatter due to inundation), vegetative growth (increasing backscatter as the canopy develops), and heading (a peak in backscatter). Applying the CR to these stages provides a compact, noise-resilient representation of the crop's progression. This enhanced temporal series is highly valuable for improving classification accuracy and pattern recognition in machine learning models such as LSTM.

3.3. Derivation of rice paddy phenology curves from Sentinel-1 and Sentinel-2 images

Accurate derivation of rice phenology curves is essential. To construct these curves, both Sentinel-1 and Sentinel-2 datasets were subjected to the preprocessing steps described in Section 3.1, thereby generating harmonized 10-day interval time series.

For Sentinel-2, the NDVI and LSWI indices were calculated over three consecutive rice-growing seasons, after which the average values across these years were computed to reduce interannual variability. Polynomial curve fitting was subsequently applied to the time-series indices, using a degree of 6 for NDVI and a degree of 3 for LSWI. These fitted functions produced smooth phenology curves that captured the seasonal dynamics of rice growth. In parallel, Sentinel-1 was used to extract the CR index over the same three years during the rice cultivation seasons, using the temporally composited 10-day data. The three-year mean CR profile was temporally aligned with the NDVI and LSWI series to maintain consistency across datasets, as illustrated in Figure 3.

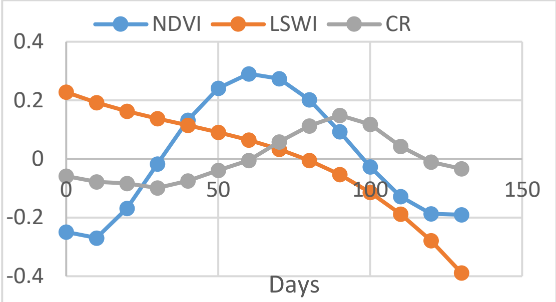

Figure 3. The LSWI and NDVI indices extracted as rice phenology curve from Sentinel-2 [28] and the CR index extracted as rice phenology curve from Sentinel-1 [29].

3.4. Feature extraction via correlation analysis

Phenology-based correlation feature extraction constitutes a critical stage in the proposed framework for accurate paddy field classification. At this stage, features are derived to characterize the temporal and phenological variations among different land cover types. Specifically, we applied a temporal correlation analysis to quantify the similarity between the phenological profile of each pixel and the proposed reference paddy phenology curve. For each pixel, time-series indices of NDVI, LSWI, and CR were first extracted. Subsequently, the correlation operation was employed to measure the similarity of each index's temporal trajectory with the paddy phenology curve over the growing season. This procedure yields a correlation curve for each index and pixel, reflecting the degree of temporal alignment between pixel-level phenological dynamics and the rice growth pattern. The correlation-based features obtained from this analysis provide more abstract and discriminative information than the raw time-series indices. From this stage, six temporal features were derived for each pixel within a 180-day period, which was divided into 18 ten-day intervals.

Time-series indices: After preprocessing, the NDVI, LSWI, and CR values were computed for each interval. These indices capture complementary information, namely vegetation health (NDVI), vegetation/soil moisture (LSWI), and surface backscatter characteristics (CR). This representation ensures that phenological dynamics from pre-planting to post-harvest, including early and late transplanting cases, are adequately covered.

Correlation-based features: To better characterize phenological similarity, the temporal profile of each index was compared with its corresponding reference paddy rice phenology curve. Specifically, a sliding window with the same length as the phenology curve (W=14) was moved along each index time series. At each window position, the mean value within the window was removed to suppress low-frequency background trends, and the similarity between the detrended time series and the phenology curve was quantified using an inner-product (cross-correlation) formulation. Formally, for each index $\in \{NDVI, LSWI, CR\}$, let $I_X(t)$ denote the value of index X at time step t (18 ten-day epochs). The windowed index vector $I_{X,t}$ is defined as:

$$I_{X,t} = \left[I_X\left(t-\frac{W}{2}\right),\dots,I_X\left(t+\frac{W}{2}-1\right)\right], \quad t = 1,\dots,18, W = 14 \tag{4}$$

Then, detrending of $I_{X,t}$ and the phenology-curve vector P_X are done as follows:

$$\tilde{I}_{X,t} = I_{X,t} - \mu_{X,t} \qquad \tilde{P}_X = P_X - \mu_{P_X} \tag{5}$$

Where $\mu_{X,t}$ and μ_{P_X} are the window-based average of $I_{X,t}$ and the average of P_X, respectively.

The correlation-based similarity score at time step t is computed as:

$$Cor_X(t) = \tilde{I}_{X,t}.\tilde{P}_X^T \qquad t = 1,\dots,18 \tag{6}$$

This procedure yields a temporal similarity sequence that $Cor_X(t)$ reflects the degree of alignment between pixel-level temporal dynamics and the characteristic rice growth pattern.

The choice of W = 14 was phenology-driven rather than arbitrary. The reference rice phenology curve represents the main rice growth cycle over 140 days, corresponding to 14 ten-day intervals. Since the complete pixel-level time series covers 180 days, the 14-step window allows the reference phenological pattern to be compared within a longer observation period and helps account for moderate shifts in planting and growth timing. A shorter window may capture only partial growth stages and become more sensitive to local fluctuations, whereas a much longer window may include excessive pre-planting or post-harvest observations and reduce sensitivity to temporal shifts. Therefore, W = 14 was selected to preserve the complete rice phenological pattern while maintaining temporal flexibility.

In total, six features were generated for each pixel: three index time series (NDVI, LSWI, and CR) and three corresponding correlation-based sequences (C_NDVI, C_LSWI, and C_CR), each represented by 18 values corresponding to the 10-day intervals. Before feature concatenation, each index time series was temporally mean-centered by subtracting its mean value. No additional min–max normalization or z-score standardization was applied. This a priori choice was based on our previous findings [29], which indicated that NDVI had a stronger phenological response and a wider correlation range than the other indices. The relative feature ranges were therefore preserved when constructing the combined input. These features were subsequently used as inputs to the LSTM model.

3.5. Development of a Deep Learning Model Based on LSTM for Mapping Rice Paddy

The LSTM-based approach demonstrated superior classification accuracy, robustness to noise, the capability to model complex temporal dependencies, and generalizability across heterogeneous landscapes [33]. These advantages underscore the strength of LSTM networks in leveraging the spatiotemporal aspect of remote sensing data for agricultural monitoring and crop mapping applications.

LSTM networks, a specialized class of Recurrent Neural Networks (RNNs), are designed to effectively model long-range temporal dependencies in sequential data, a domain where traditional RNNs are often inadequate. The critical limitation of traditional RNNs is the vanishing gradient problem, which impedes the flow of error signals through many time steps during backpropagation, thereby preventing effective learning of long-term contextual relationships. LSTMs are equipped with a gating mechanism (input, output, and forget gates) that allows them to selectively retain, update, or discard information over long sequences. This mechanism enables LSTMs to learn both short- and long-term dependencies within time series data.

The core component of the LSTM architecture is the memory cell that retains the cell state over time, regulated by the three aforementioned adaptive gates. In a typical LSTM-based model, the time-series input is first passed through one or more LSTM layers, which learn and extract relevant sequential features from the data. These features are subsequently processed by dropout and dense (fully connected) layers to perform classification or regression tasks. In the final stage, paddy field mapping was carried out using the extracted features (NDVI, LSWI, CR, and their correlation-based counterparts C_NDVI, C_LSWI, C_CR) as inputs to an LSTM neural network.

4.Experiment Design

4.1. LSTM Training and Mapping

The LSTM architecture was developed using the Keras API on the TensorFlow machine learning framework and implemented in Python. The LSTM model was designed to handle the extended time series and full correlation features as follows:

- **Input Layer:** Each pixel sample was represented as a temporal sequence with 18-time steps, corresponding to 18 ten-day intervals over the 180-day observation period. The number of features per time step depended on the evaluated feature set. For the raw time-series indices, the input shape was (18, 3), including NDVI, LSWI, and CR. For the correlation-based features, the input shape was also (18, 3), including C_NDVI, C_LSWI, and C_CR. For the combined representation, the input shape was (18, 6), including NDVI, LSWI, CR, C_NDVI, C_LSWI, and C_CR. Thus, the LSTM input tensor was organized as (number of samples, 18, F), where F denotes the number of input features.
- **LSTM Layer:** Consists of 16 units, followed by a dropout layer (rate=0.3) for regularization, given the increased sequence length and limited training data.
- **Dense Layer:** A fully connected layer with 8 units, ReLU activation, and L2 regularization (λ=0.01), followed by a dropout layer (rate=0.3).
- **Output Layer: A single unit with a sigmoid activation function for binary classification (Rice vs. Non-Rice).**

The architecture with a reduced number of LSTM units and a higher dropout rate captures essential temporal patterns without overfitting. Figure 4 depicts the structural design of the model.

4.2. Evaluation Metrics

To assess the three classification methods, the following key evaluation metrics were computed and compared: Overall Accuracy (OA), Precision (P), Recall (R), and F1-Score, which are derived from the counts in the confusion matrix.

True Positives (TP): The number of actual positive samples correctly classified as positive.

- True Negatives (TN): The number of actual negative samples correctly classified as negative.
- False Positives (FP): The number of actual negative samples incorrectly classified as positive (Type I error).
- False Negatives (FN): The number of actual positive samples incorrectly classified as negative (Type II error).

Overall Accuracy (OA): Measures the overall performance of the classifier across all classes and is calculated as:

$$Overall \quad Accuracy = \frac{TP + TN}{Total \quad samples} \tag{7}$$

Precision (P): Indicates the proportion of correctly predicted positive samples among all samples predicted as positive.

$$Precision = \frac{TP}{TP + FP} \tag{8}$$

$$Recall = \frac{TP}{TP + FN} \tag{9}$$

F1-Score: The harmonic means of Precision and Recall, providing a balance between these two metrics.

$$F1 - Score = \frac{Precision \times Recall}{Precision + Recall} \times 2 \tag{10}$$

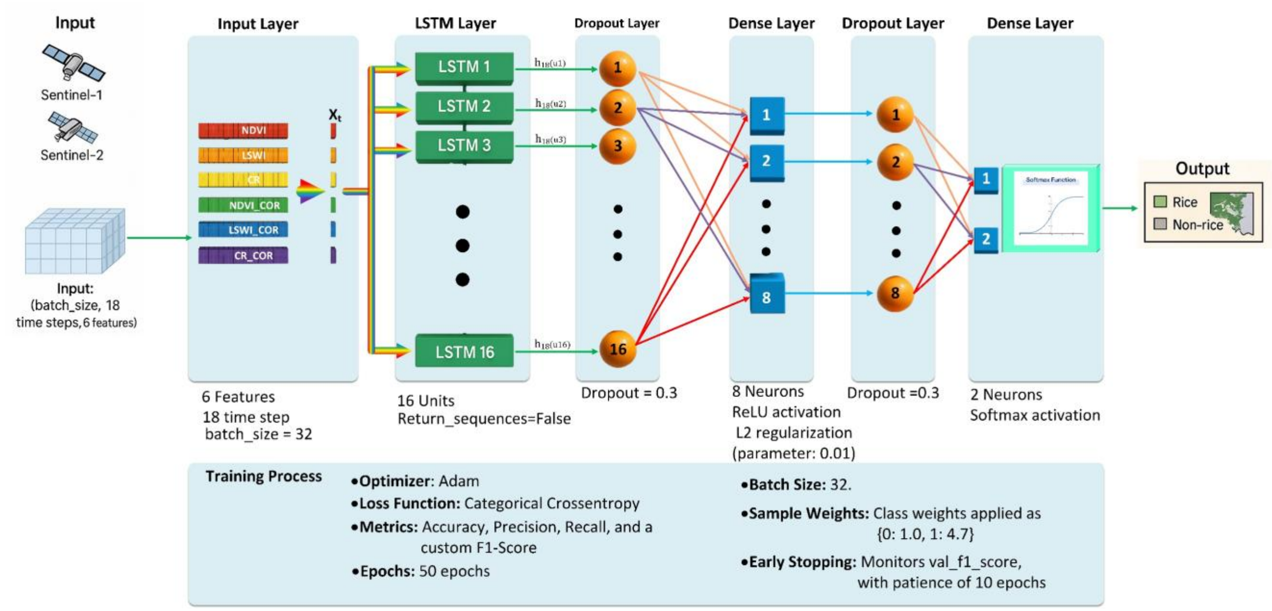

Figure 4. The structure of the proposed LSTM model.

5. Evaluation and Results

To assess the impact of different types of input features on the proposed model's performance, three distinct feature sets were designed for training and evaluation. The objective was to determine the most effective combination of primary indices and derived temporal correlation-based features for accurately discriminating rice paddies from other land-cover types. The following feature sets were designed and tested:

- Feature Set 1: Comprised the raw time series of three key indices, NDVI, LSWI, and CR, during the growing season.
- Feature Set 2: Consisted of three correlation-based features (C_NDVI, C_LSWI, and C_CR), derived from the correlation between each index's time series (NDVI, LSWI, CR) and the corresponding rice phenology curve. This set represents the temporal similarity between a pixel's index time series and the reference rice phenological profile.
- Feature Set 3: A combined feature set, including both the raw time series indices from Set 1 and the correlation-based features from Set 2.

Field data partitioning: The study was conducted in an area with diverse land-cover types, including rice paddies, orchards, other agricultural fields, urban areas, and water bodies. The rice growth cycle in the region typically ranges from 90 to 120 days but varies depending on cultivar and farming practices. Early planting can occur due to successive cropping, while late planting may result from crop rotation. To capture this variability, the rice phenology curve was constructed over a 140-day period (with 14 ten-day intervals), covering pre-planting flooding through post-harvest stages. Correspondingly, satellite image time series were extracted over a 180-day period (with 18 ten-day intervals) to ensure coverage of all potential growth cycles.

Model training and evaluation: A total of 50 labeled polygons were used for model development, and 109 polygons were reserved for independent testing. The model-development set contained 16,269 samples, which were further divided into 13,015 training samples and 3,254 validation samples using an 80:20 split. The independent test set contained 49,238 samples and was used only for the final evaluation. To address class imbalance (a non-paddy to paddy ratio of approximately 4.7:1), class weighting was applied during training.

Ablation and sensitivity analysis: To evaluate the contribution of the main input representations, three feature sets were compared under the same LSTM-based framework: raw time series indices, correlation-based features, and their combined representation. In addition, several LSTM configurations with different numbers of units, dense-layer sizes, and dropout rates were trained and evaluated to assess the effect of model complexity and regularization. The sliding-window length was set to W = 14 because the reference rice phenology curve covered the main rice growth cycle over 14 ten-day intervals. Similarly, the 10-day temporal resolution was selected as a compromise between preserving phenological details and reducing missing observations caused by cloud contamination. Although the feature set and dropout/model configuration analyses were experimentally evaluated.

In Table 2, the performance of the model based on each feature set was evaluated on the test set using standard metrics, including overall accuracy, precision, recall, and F1 score. In addition, the confusion matrices corresponding to different feature sets are presented in Tables 3 to 5 for detailed analysis of classification performance.

Table 2. Comparison of the performance of the proposed method based on different features.

	Overall Accuracy (%)	Precision (%)	Recall (%)	F1-score (%)
Raw time-series indices (NDVI, LSWI, CR)	99.06	99.42	95.59	97.46
Correlation-based features (C_NDVI, C_LSWI, C_CR)	**99.81**	99.61	**99.40**	**99.50**
Combined raw and correlation-based features	99.21	**99.82**	95.97	97.86

Table 3. Confusion matrix for the evaluation set for three time series indices (NDVI, LSWI and CR).

	Predicted Rice	Predicted Non-Rice
Actual Rice	8862	409
Actual Non-Rice	52	39915

Table 4. Confusion matrix for the evaluation set for three time series of correlation indices (C_NDVI, C_LSWI and C_CR).

	Predicted Rice	Predicted Non-Rice
Actual Rice	9215	56
Actual Non-Rice	36	39931

Table 5. Confusion matrix for the evaluation set for 6 features (three indicators and three indicator correlations).

	Predicted Rice	Predicted Non-Rice
Actual Rice	8897	374
Actual Non-Rice	16	39951

The performance analysis of the three feature sets for rice paddy mapping demonstrated that Feature Set 2 (correlation series: C_NDVI, C_LSWI, C_CR) achieved the best results, with 36 false positives (FP) and 56 false negatives (FN), totaling 92 errors (i.e., error rate = 0.19%). This set reached an overall accuracy of 99.81%, an F1-score of 0.9950, and a recall of 0.99 for the rice class. Its superior performance is attributed to the correlation operation, which effectively reduced low-frequency noise (e.g., atmospheric effects and variations before planting and after harvest) while highlighting key phenological stages (e.g., flooding, vegetative, reproductive, ripening). As a result, rice paddies were accurately identified even in challenging areas involving diverse planting schedules or proximity to water bodies.

In contrast, Feature Set 1 (raw indices: NDVI, LSWI, CR) performed the worst, with 461 total errors (52 FP and 409 FN) and an error rate of 0.94%. The absence of correlation-based features limited its ability to capture complex temporal growth patterns. The high FN count (recall = 0.96) indicated a fundamental weakness in distinguishing rice paddies from land covers with similar spectral responses, particularly in water-dominated areas with high LSWI during the flooding stage.

Feature Set 3 (combined raw indices and correlation-based features) showed intermediate performance, with 390 errors (16 FP and 374 FN) and a 0.79% error rate. While it outperformed Feature Set 1, the inclusion of noisy raw indices increased FN errors (4.0% of rice samples), despite achieving very low FP (0.04%), which reflected high precision. Spatial error analysis revealed that FN errors in both Feature Sets 1 and 3 were concentrated in areas of strong spectral similarity, whereas Feature Set 2 substantially mitigated these issues by focusing on temporal patterns.

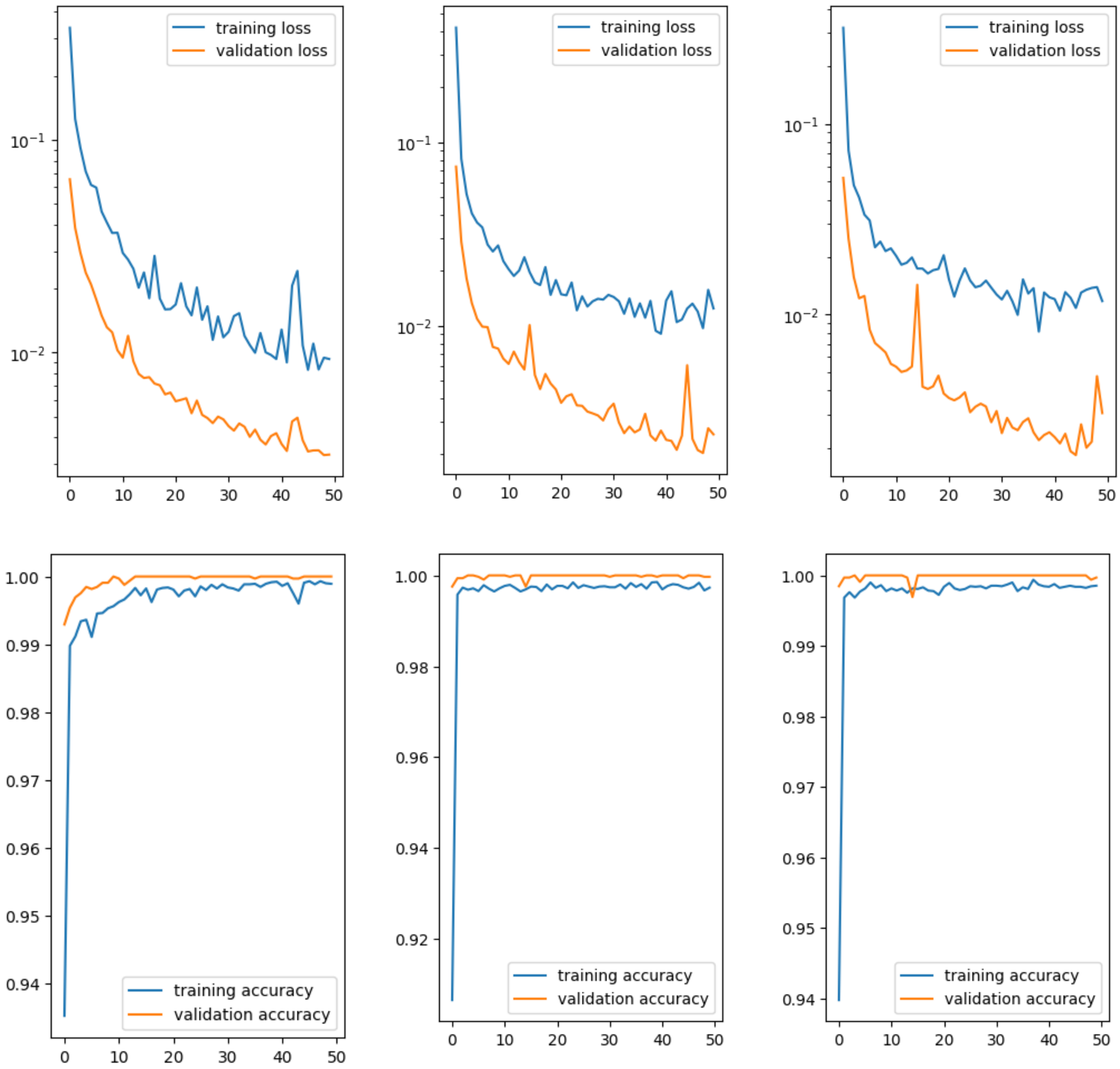

(a) (b) (c)

Figure 5. Training and Validation curves (a) Three time series indices (NDVI, LSWI and CR), (b) Three correlation-based features (C_NDVI, C_LSWI and C_CR), (c) set for 6 features (three time-series indices and three correlation-based features).

Overall, the proposed method's high accuracy stems from the integration of robust preprocessing (10-day quantization and interpolation of missing data), phenology-based feature extraction that captures essential growth dynamics, and the LSTM model capable of learning long-term temporal dependencies. The use of class weighting to address the 4.7:1 class imbalance and early stopping to avoid overfitting ensure a reliable and practically applicable model for precision agriculture and paddy field monitoring.

To evaluate the model's learning behavior and generalization capability, the evolution of training and validation accuracy and loss was analyzed. Figure 5 compares these metrics across three experimental configurations: (a) using time-series indices (NDVI, LSWI, and CR), (b) employing correlation-based features (C_NDVI, C_LSWI, and C_CR), and (c) utilizing an integrated set of all six features. To compare the three feature categories, we trained a suite of LSTM variants and evaluated their performance. Model names encode the architecture as follows: LSTM<units>-<layers>L-D<dense>-D<dropout>. For example, LSTM16-1L-D8-D0.3 has 16 LSTM units, one LSTM layer, an 8-unit dense layer, and a dropout rate of 0.3.

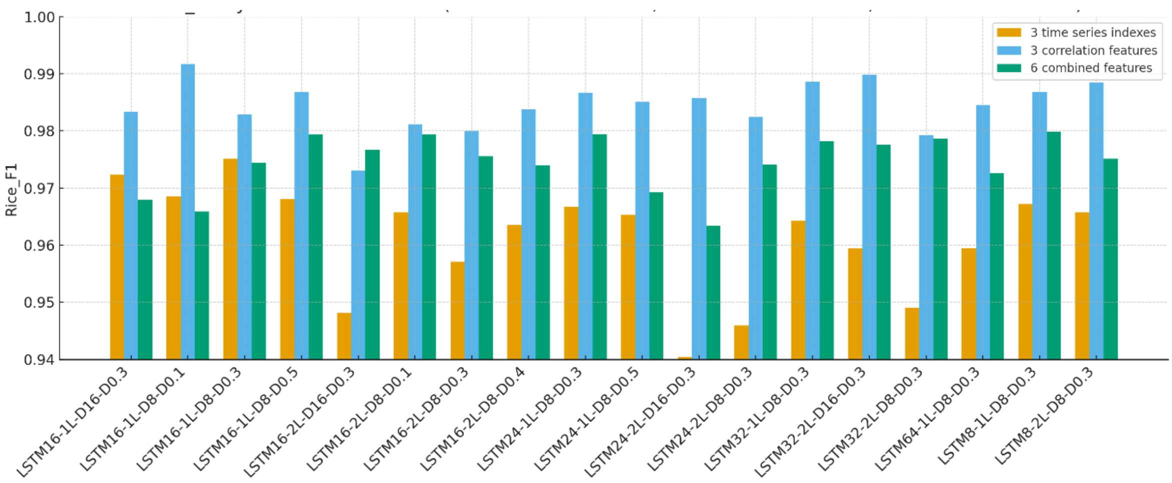

Figure 6. Rice_F1 of the LSTM models for the three feature sets.

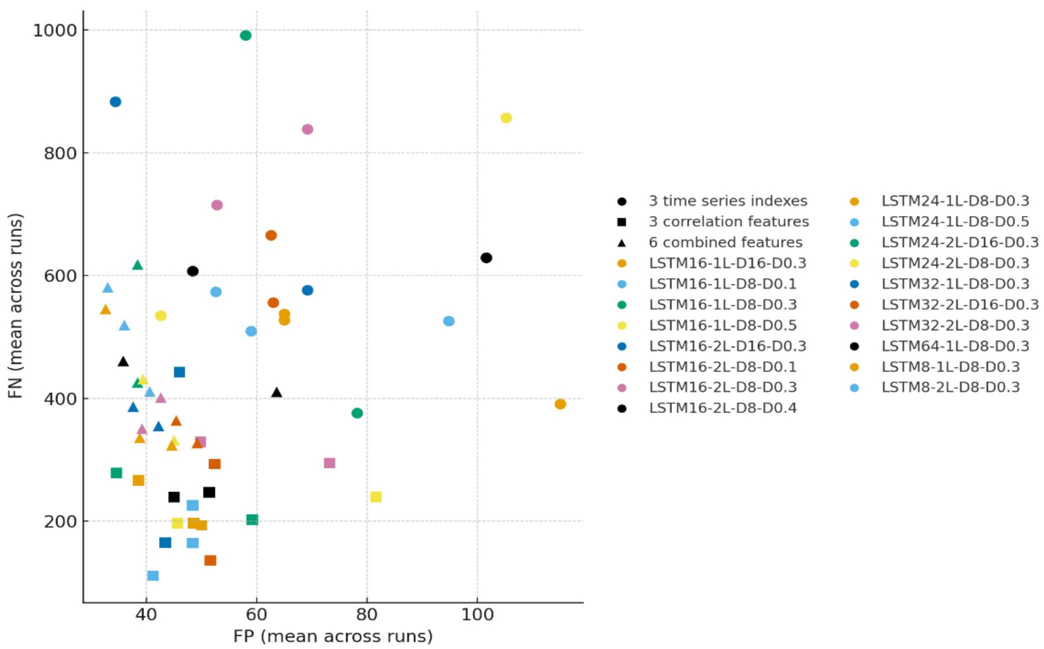

Figure 7. False Positives (FP) versus False Negatives (FN) for the three feature sets.

Models were compiled with Adam and categorical cross-entropy and monitored using accuracy, precision, recall, AUC-ROC (Area Under the ROC Curve), and AUPRC (Area Under the Precision–Recall Curve). We trained for up to 50 epochs and applied Early Stopping on AUPRC to prevent overfitting. The number of epochs was large enough to ensure that training completion for each model was determined by Early Stopping. To address class imbalance, we used sample weights {0: 1.0, 1: 4.71}. The results of a model change slightly with each run because some random processes are involved in training the model, so to obtain more comparable results, each model was trained five times for each feature set.

We report the mean confusion counts (TN, FP, FN, TP) and derive accuracy (%), Kappa, rice-class precision/recall/F1, mIoU (mean IoU over rice and non-rice), and balanced accuracy from the mean counts. Figure 6 plots Rice_F1 across models for the three groups. Figure 7 shows mean FP vs. FN for each model. The correlation-feature group generally clusters closer to the origin, indicating lower error rates. Table 6 lists the best identified model for each feature set based on the Rice F1 scale, along with accuracy (%), kappa, Rice F1 (%), mIoU (%), balanced accuracy (%), and mean confusion count.

Table 6. Best model by feature set (mean over 5 runs).

Feature set	Best model	Accuracy (%)	Kappa	Rice F1 (%)	mIoU (%)	Balanced Acc. (%)	TN	FP	FN	TP
Time series indices	LSTM16-1L-D8-D0.3	99.08	0.9694	97.51	97.01	97.87	39888.8	78.2	376.0	8895.0
Correlation features	LSTM16-1L-D8-D0.1	99.69	0.9898	99.17	98.99	99.35	39925.8	41.2	111.4	9159.6
combined features	LSTM8-1L-D8-D0.3	99.25	0.9753	97.98	97.57	98.20	39922.4	44.6	323.6	8947.4

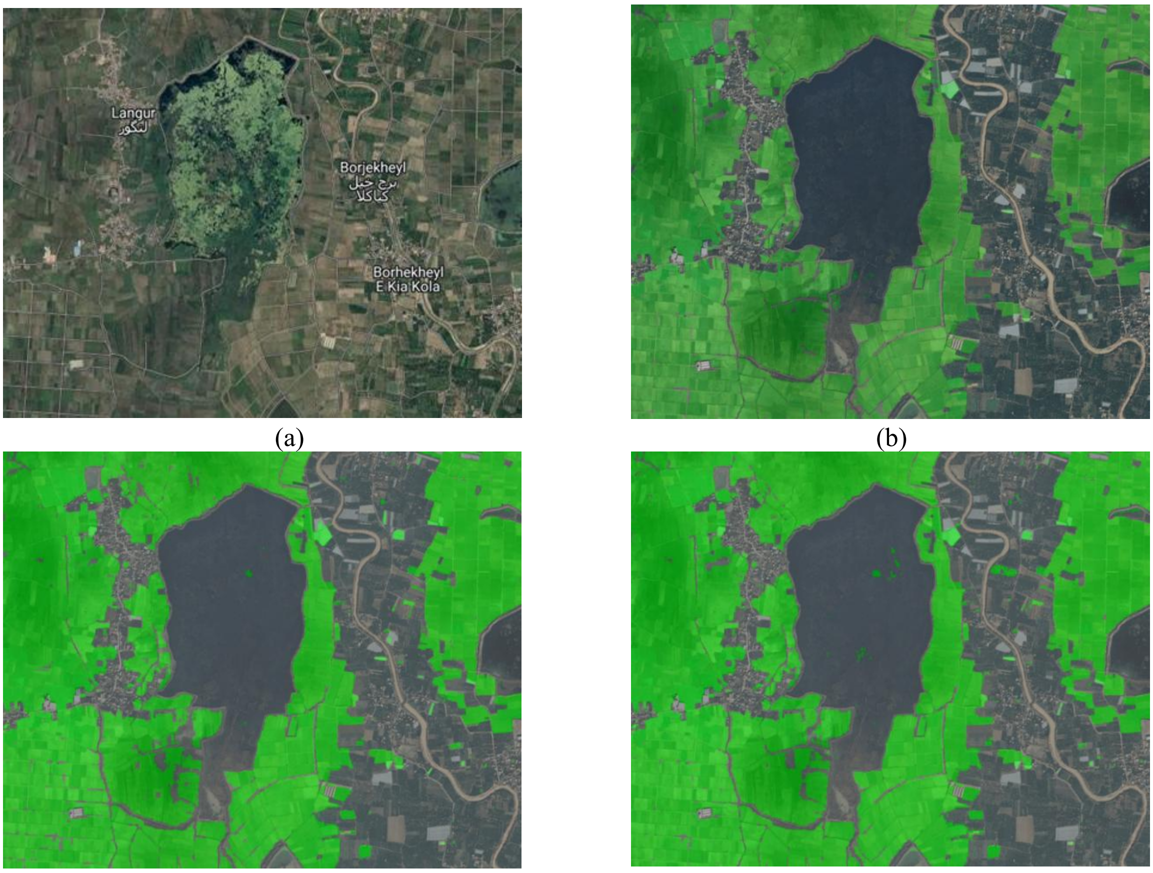

Figure 8: (a) Part of the study area, Mapping of rice fields using different features in 2024: (b) three time series indices (NDVI, LSWI and CR), (c) three time series of correlation indices (C_NDVI, C_LSWI and C_CR), (d) set for 6 features (three indicators and three indicator correlations).

In Figure 8(b), the mapping was performed using only the three raw time series indices (NDVI, LSWI, and CR). As shown, the model using this feature set achieved a relatively successful discrimination between rice fields, other agricultural lands, and residential areas. However, a portion of the reservoir was misclassified as rice fields, highlighting the limitations of the raw time series indices in separating these two land cover types. In contrast, the mapping generated using the second feature set (Figure 8(c)) and the third feature set (Figure 8(d)) shows a significant improvement in distinguishing weeds from rice fields. This demonstrates that correlation-based features provide richer and more distinct information than raw time series indices. These findings emphasize the importance of employing advanced preprocessing and higher-level feature extraction techniques for vegetation classification in complex landscapes. A similar evaluation was conducted for an additional test area (Figure 9), and the results exhibited the same overall trend.

To visually evaluate the effectiveness of the proposed approach, a subset of the study area is illustrated in Figure 10(a).

This area consists of small and scattered agricultural fields. Figure 10(b) shows the hand-drawn rice fields obtained through visual interpretation, while Figure 10(e) presents the rice field mapping results generated using the three correlation-based indices as inputs to the LSTM model. Due to the small size of the fields and the ratio between the field dimensions and the pixel size of the Sentinel-1 and Sentinel-2 images, a significant number of pixels lie along the boundaries between different land cover types and thus contain mixed spectral information. This spectral mixing complicates the accurate discrimination of adjacent fields. Nevertheless, the proposed method shows satisfactory mapping performance despite these challenges.

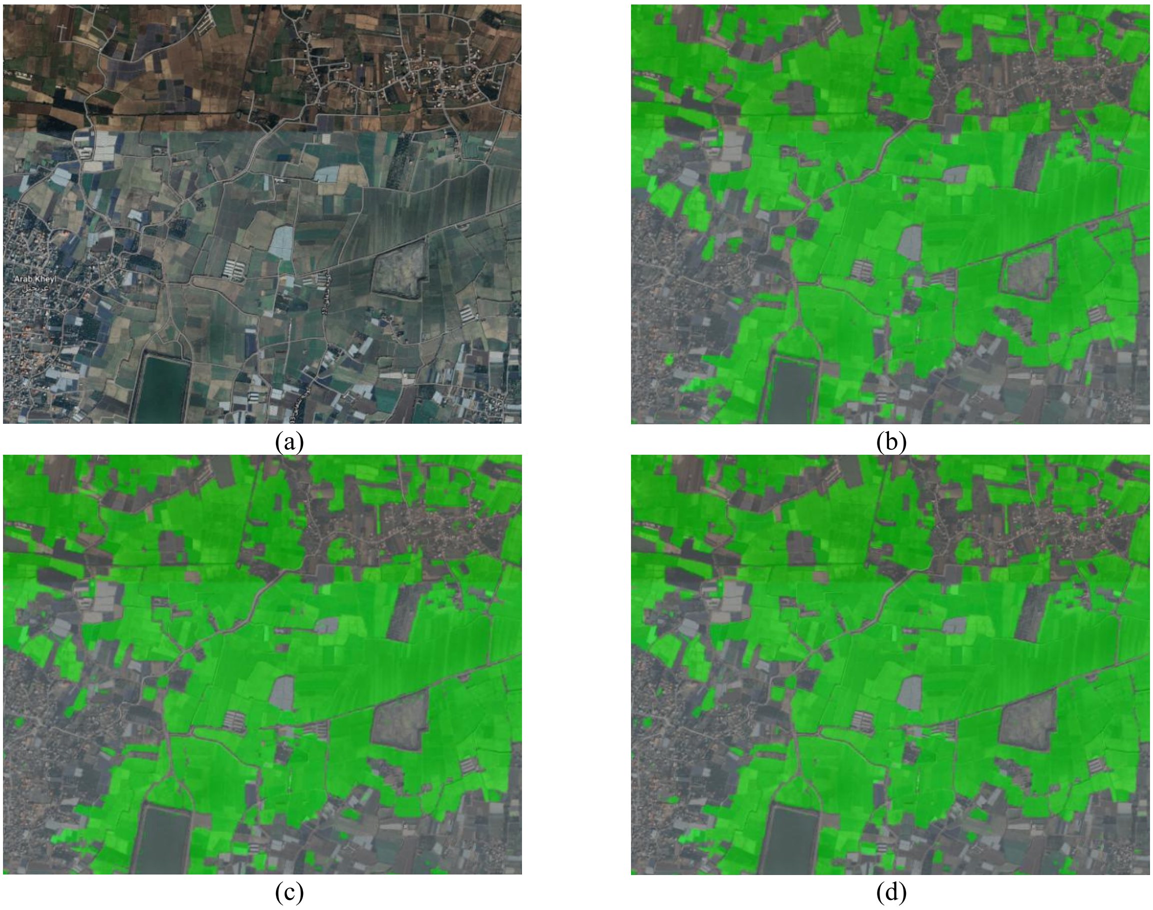

Figure 9: (a) Part of the study area, Mapping of rice fields using different features in 2024: (b) three time series indices (NDVI, LSWI and CR), (c) three time series of correlation indices (C_NDVI, C_LSWI and C_CR), (d) set for 6 features (three indicators and three indicator correlations).

Furthermore, the edges in Figure 10(e) appear less smooth compared to those in Figure 10(b) because Figure 10(b) was generated from high-resolution images, while the data used in Figure 10(e) were extracted from Sentinel-1 and Sentinel-2 satellite images with lower spatial resolution.

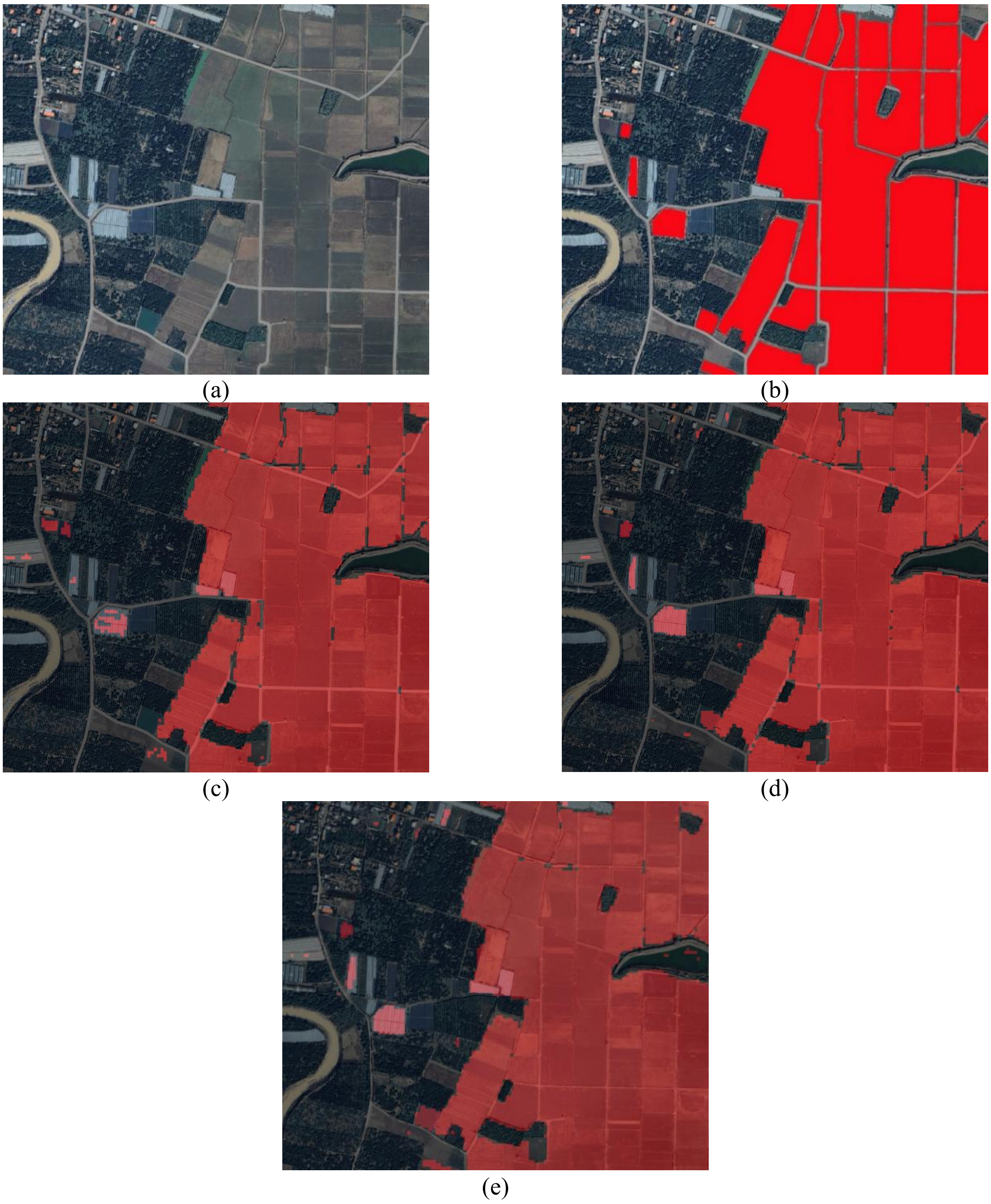

Figure 10. Visual evaluation of paddy field mapping performance in 2024. Proposed method, (a) a subset of the study area; (b) Depicting rice fields in red through visual interpretation, (c) Results of mapping rice fields proposed [28], (d) Results of mapping rice fields proposed [29], (e) Results of mapping rice fields using the proposed method.

6. Discussion

Rice paddies exhibit intricate planting arrangements and considerable environmental variability, which present substantial obstacles for precise mapping of rice cultivation areas. Traditional machine learning methods (e.g., DT, RF, and SVM) often encounter limitations when applied to such heterogeneous landscapes. These methods rely on features that may be derived manually using expert knowledge or through data mining and image processing techniques. However, the inherent complexities of planting patterns and the environmental variability of rice paddies, including variations in soil conditions, climate, and agricultural practices, limit the accuracy and efficiency of these methods. Consequently, there is a pressing need for more advanced methodologies, such as deep learning or the integration of multi-source data, to improve mapping accuracy by capturing the intricate spatiotemporal dynamics of rice cultivation. In recent years, deep learning models have emerged as powerful tools for crop mapping. CNNs, which learn spatial features from satellite imagery, have demonstrated superior performance in agricultural crop classification compared to traditional classification methods [34]. Additionally, RNNs have shown considerable promise in rice classification by autonomously extracting temporal features from time-series satellite imagery. Long Short-Term Memory (LSTM) networks, a specialized type of RNN, are particularly effective at modeling temporal dependencies within sequential data [35].

The Bidirectional LSTM (BiLSTM) incorporates dual-directional temporal processing, which facilitates a more comprehensive assimilation of contextual dependencies within sequential data [36]. Compared to Transformer architectures, which rely on self-attention and necessitate large-scale datasets and significant computational power, LSTM and BiLSTM networks provide a more practical and computationally efficient means of capturing temporal dependencies in sequential data [37]. Advanced hybrid models have also been developed for paddy field mapping. For instance, the ConvLSTM-RFC model [38] integrates features from RNN and CNN to leverage both spatial and temporal features for mapping rice cultivation areas using Sentinel-1 radar imagery, achieving high classification performance. Additionally, an attention mechanism is employed to assign greater weight to more informative time steps, enabling the model to focus on critical growth stages, such as the flooding stage or rapid vegetative growth. To address class imbalance and reduce sensitivity to outliers, a focal loss function was applied, emphasizing harder-to-classify samples. Regularization techniques were also incorporated to mitigate overfitting. This combined approach enabled the model to achieve an overall accuracy of 98.08% with a false positive rate of 15.08%.

RiceLSTM and RiceTS were proposed for mapping paddy fields [39]. RiceLSTM is based on a BiLSTM architecture with an Attention mechanism to extract temporal dependencies from radar time-series data, while RiceTS combines U-Net and MobileNetV2 to incorporate spatial and temporal information. Both models achieved high accuracy (approximately 96–98%) on Hainan Island datasets. However, the performance of such data-driven models depends on two critical factors. First, they rely on a large volume of high-quality and representative training data to achieve both accuracy and generalizability in paddy rice mapping with deep learning algorithms. Second, they depend on complete and consistent temporal observations. Gaps or irregularities in time-series data can substantially affect model reliability, particularly for deep learning approaches that depend on temporal backscattering patterns to characterize rice growth dynamics. Precise delineation of paddy rice fields relies on effectively capturing critical phenological stages, including transplanting, tillering, and maturation [40]. Missing data during essential growth stages impair the model's ability to accurately represent paddy rice dynamics and often lead to misclassification, particularly when distinguishing rice from other vegetation types with similar scattering characteristics, such as wetland vegetation, rainfed crops, or water bodies [18].

A further persistent challenge involves the misidentification of wetland vegetation as paddy rice fields, owing to similarities in backscattering properties, temporal scattering variations, vegetation structures, and geographic overlap. The resemblance of backscatter signals complicates the discrimination between rice and wetland vegetation, which in turn increases the likelihood of misclassifying paddy rice fields [18].

In this study, a framework was developed for paddy rice mapping by integrating multi-sensor time-series imagery from both radar and optical satellite platforms within an LSTM-based deep learning architecture. The proposed approach demonstrated that incorporating both spectral indices (NDVI, LSWI, CR) and their temporal correlations with rice phenological patterns significantly enhances classification accuracy at the pixel level. Unlike traditional methods that rely on static thresholds or single-date features, our correlation-based indices (C_NDVI, C_LSWI, C_CR) captured dynamic temporal similarities between individual pixels and the phenology curve, thereby improving the model's ability to distinguish rice paddies from spectrally or structurally similar land covers.

The results highlight the critical role of complete and continuous time-series data, particularly during key phenological stages such as transplanting, tillering, and maturation, in achieving reliable mapping performance. This finding aligns with recent studies emphasizing the importance of temporal continuity for crop monitoring. Furthermore, the integration of radar and optical indices proved advantageous, as radar backscatter captured water-related dynamics during the flooded and transplanting phases, while optical indices provided complementary information on vegetation growth.

Despite the promising results, the proposed framework remains dependent on the availability of high-quality training samples and consistent temporal data coverage. Data gaps during critical phenological windows still pose challenges, potentially leading to misclassification, especially between rice paddies and wetland vegetation with similar scattering characteristics. Future work should therefore focus on developing data augmentation strategies, incorporating multi-year training samples, and exploring self-supervised learning approaches to reduce reliance on extensive ground truth data.

This study presents a novel and highly accurate framework for rice paddy mapping by integrating multi-temporal radar and optical satellite imagery with an LSTM-based deep learning model. The framework utilizes rice phenology, time series learning, and advanced satellite image processing to achieve high-accuracy pixel-level identification of rice fields. The pre-processing step included cloud removal, temporal quantization at 10-day intervals, and interpolation of missing observations, resulting in smooth and analyzable time series data. Subsequently, vegetation and moisture indices including Sentinel-2-derived NDVI and LSWI and Sentinel-1-derived CR were extracted over the entire rice growth cycle. To capture phenological similarity, temporal correlations between reference rice phenology curves and pixel time series were calculated, resulting in the correlation features C_NDVI, C_LSWI, and C_CR. These features quantified the extent to which the temporal behaviour of each pixel conformed to the typical rice growth pattern. Finally, an LSTM model was designed and trained using three different feature sets (raw indices, correlation-based indices, and a hybrid set), with optimized settings including dropout, class weighting, and early stopping to ensure robust learning.

The results of testing the proposed LSTM model on three types of feature inputs show that the type of feature has a direct and significant impact on the final classification accuracy. Below are some key points extracted from the model comparison:

1. **Superiority of Phenology-Correlation Features**

Features derived from the correlation between the rice phenology curve and the pixel-based time series indices (C_NDVI, C_LSWI, and C_CR) achieved the best performance. An F1-Score of 0.9950 and an overall accuracy of 0.9981 highlight the model's exceptional ability to distinguish rice fields from non-rice areas. These results indicate that the model not only performed well in identifying the majority class (non-rice) but also exhibited outstanding reliability in detecting the minority class (rice).

2. **Limitations of Raw Time-Series Indices**

Although the raw time-series indices (NDVI, LSWI, and CR) provide valuable information on vegetation condition and surface moisture, their classification performance was inferior to that of the correlation-based features. With an F1-Score of 0.9746, the model was more prone to false negatives, meaning that some rice pixels were misclassified as non-rice. This limitation arises from the spectral similarity of rice fields during certain growth stages with other land covers such as grasslands, seasonal crops, or water bodies.

3. **Behavior of Combined Features**

Although the combined feature set performed better than the raw indices alone, it did not outperform the correlation-only features. The correlation transformation provides a compact representation that emphasizes similarity to the rice phenological pattern while reducing short-term fluctuations and background variations. Adding the raw NDVI, LSWI, and CR series reintroduced partly redundant and less discriminative information and increased the input dimensionality from three to six features. With the available training data, this additional complexity did not improve the model's generalization. This behavior is also evident in the confusion matrices: the combined feature set reduced the number of false positives from 36 to 16, but increased the false negatives from 56 to 374. It therefore achieved slightly higher precision but lower recall and F1-score than the correlation-only feature set.

Overall, the results demonstrate that the similarity between each pixel's time series and the reference phenology curve of rice (correlation-based features) is a highly discriminative indicator for paddy field mapping. In this study, by applying 10-day temporal quantization and gap-filling through interpolation, uniform and complete time series were constructed. Subsequently, correlation between each pixel's indices and rice phenology curves was calculated, producing robust features that not only enriched the information content but also inherently acted as a filter to substantially reduce noise. Finally, with the optimized LSTM model, an overall accuracy of 99.81% was achieved. The proposed framework was implemented in the cloud-based environment of Google Colab, using Python, TensorFlow, and Keras, as well as the Google Earth Engine (GEE) API for large-scale data processing.

4. **Model complexity and architecture selection:**

A compact single-layer LSTM was selected to balance temporal modeling capability and model complexity. The input sequence contained only 18 ten-day observations, and the correlation-based features already incorporated phenological prior knowledge by representing the similarity between pixel-level temporal trajectories and reference rice phenology curves. Therefore, a more complex architecture such as BiLSTM or an attention-based model was not necessary for capturing the main temporal dependencies in this study and could increase the risk of overfitting with the available imbalanced training data. Nevertheless, such advanced architectures may be useful for larger datasets, longer time series, or multi-region transfer experiments.

5. **Sensitivity to interpolation and cloud contamination:**

The proposed framework relies on complete and temporally consistent time series; therefore, interpolation quality and cloud contamination can affect the reliability of the extracted features. In this study, these effects were mitigated by applying 10-day temporal compositing before interpolation, using correlation-based features that emphasize the overall phenological trajectory rather than isolated observations, and integrating the Sentinel-1-derived CR feature, which provides cloud-insensitive complementary information to Sentinel-2 optical indices. Nevertheless, the method is not fully immune to severe and persistent cloud contamination. Long consecutive gaps in Sentinel-2 observations, especially during key phenological stages such as flooding, transplanting, tillering, or heading, may distort the reconstructed NDVI and LSWI profiles and reduce classification performance.

6. **Generalization to other rice-growing regions:**

Although the proposed framework was evaluated in Mazandaran Province, it has potential transferability because it relies on general rice phenological behaviour and globally available Sentinel-1 and Sentinel-2 observations. The correlation-based features focus on the temporal similarity between pixel-level index trajectories and the reference rice phenology curve, rather than only on absolute spectral values, which can improve robustness to moderate local radiometric variations and noise. However, differences in rice cultivars, cropping calendars, and the timing of key phenological stages may affect direct application to new regions. Therefore, the reference phenology curves should be recalibrated using representative local or regional samples, and the LSTM model may require fine-tuning when the target region has substantially different phenological patterns.

7. Conclusion

In this study, we developed a comprehensive and high-accuracy rice-mapping approach by integrating SAR (Sentinel-1) and optical Earth observation data (Sentinel-2) with an LSTM neural network. The proposed approach, through careful design of pre-processing, index extraction, rice phenology curve derivation, and the integration of time-series information with phenology-based correlation features, achieved highly accurate classification of rice pixels using real-world datasets. Among the tested feature sets, correlation-based features showed superior discriminative power, underscoring that explicitly encoding phenological information significantly improves spatial classification performance in temporally structured agricultural landscapes.

The LSTM model, as a powerful recurrent network for time-series analysis, effectively captured the temporal patterns of vegetation indices in this study. Moreover, when faced with imbalanced data (large ratio of non-rice to rice pixels), the use of class weighting and early stopping successfully maintained balanced recognition across both categories.

The comprehensive evaluation conducted in this study confirms that:

- Temporal sequences of satellite imagery, when properly pre-processed and standardized, can accurately capture the dynamics of crop growth.
- Incorporating phenological curve information of rice enhances classification performance while simultaneously improving the model's robustness and transferability across different growing seasons and regions.
- Deep learning models such as LSTM, when combined with well-designed architectures, high-quality datasets, and fine-tuning strategies, are powerful tools for precision agriculture and large-scale crop monitoring.

References

[1] N. Kussul, S. Drozd, H. Yailymova, A. Shelestov, G. Lemoine, and K. Deininger, "Assessing damage to agricultural fields from military actions in Ukraine: An integrated approach using statistical indicators and machine learning," *International Journal of Applied Earth Observation and Geoinformation,* vol. 125, p. 103562, 2023.

[2] M. Singha, J. Dong, G. Zhang, and X. Xiao, "High resolution paddy rice maps in cloud-prone Bangladesh and Northeast India using Sentinel-1 data," *Scientific data,* vol. 6, no. 1, p. 26, 2019.

[3] J. Dong, X. Xiao, M. A. Menarguez, G. Zhang, Y. Qin, D. Thau, ... & B. Moore III, (2016). Mapping paddy rice planting area in northeastern Asia with Landsat 8 images, phenology-based algorithm and Google Earth Engine. *Remote sensing of environment*, *185*, 142-154.

[4] G. Zhang, X. Xiao, J. Dong, F. Xin, Y. Zhang, Y. Qin, RB. Doughty and *B. Moore III.*, "Fingerprint of rice paddies in spatial–temporal dynamics of atmospheric methane concentration in monsoon Asia," *Nature communications,* vol. 11, no. 1, p. 554, 2020.

[5] H. Yang, B. Pan, N. Li, W. Wang, J. Zhang, and X. Zhang, "A systematic method for spatio-temporal phenology estimation of paddy rice using time series Sentinel-1 images," *Remote Sensing of Environment,* vol. 259, p. 112394, 2021.

[6] L. Pan, H. Xia, X. Zhao, Y. Guo, and Y. Qin, "Mapping winter crops using a phenology algorithm, time-series Sentinel-2 and Landsat-7/8 images, and Google Earth Engine," *Remote sensing,* vol. 13, no. 13, p. 2510, 2021.

[7] Y. He, J. Dong, X. Liao, L. Sun, Z. Wang, N. You, Z. Li and P. Fu, "Examining rice distribution and cropping intensity in a mixed single-and double-cropping region in South China using all available Sentinel 1/2 images," *International Journal of Applied Earth Observation and Geoinformation,* vol. 101, p. 102351, 2021.

[8] C. Huang, S. You, A. Liu, P. Li, J. Zhang, and J. Deng, "High-Resolution National-Scale Mapping of Paddy Rice Based on Sentinel-1/2 Data," *Remote Sensing,* vol. 15, no. 16, p. 4055, 2023.

[9] G. Tian, H. Li, Q. Jiang, B. Qiao, N. Li, Z. Guo, J. Zhao and H. Yang, "An Automatic Method for Rice Mapping Based on Phenological Features with Sentinel-1 Time-Series Images," *Remote Sensing,* vol. 15, no. 11, p. 2785, 2023.

[10] A.-X. Zhu, F.-H. Zhao, H.-B. Pan, and J.-Z. Liu, "Mapping rice paddy distribution using remote sensing by coupling deep learning with phenological characteristics," *Remote sensing,* vol. 13, no. 7, p. 1360, 2021.

[11] S. Liang, Y. Chen, J. Liu, H. Ma, W. Li, P. Sucharitakul, N. Luo, Z. Chen, H. Fang, F. Zhang and J. Xu, "Mapping paddy rice cropping intensity and calendar in monsoon asia at 20 m resolution between 2018 and 2021 from multi-source satellite data using a sample-free algorithm," *Available at SSRN 4948283,* 2024.

[12] D. Huang, L. Xu, S. Zou, B. Liu, H. Li, L. Pu and H. Chi, "Mapping Paddy Rice in Rice–Wetland Coexistence Zone by Integrating Sentinel-1 and Sentinel-2 Data," *Agriculture,* vol. 14, no. 3, p. 345, 2024.

[13] Q. Jiang, Z. Tang, L. Zhou, G. Hu, G. Deng, M. Xu and G. Sang, "Mapping Paddy Rice Planting Area in Dongting Lake Area Combining Time Series Sentinel-1 and Sentinel-2 Images," *Remote Sensing,* vol. 15, no. 11, p. 2794, 2023.

[14] L. Sun, T. Yang, Y. Lou, Q. Shi, and L. Zhang, "Paddy rice mapping based on phenology matching and cultivation pattern analysis combining multi-source data in Guangdong, China," *Journal of Remote Sensing,* vol. 4, p. 0152, 2024.

[15] X. Jiang, S. Gao, H. Du, S. Fang, Y. Gong, N. Han and Y. Wang, "An automatic decision-level fusion rice mapping method of optical and SAR images based on cloud coverage," *IEEE Journal of Selected Topics in Applied Earth Observations and Remote Sensing,* 2025.

[16] V. N. Fikriyah, R. Darvishzadeh, A. Laborte, and A. Nelson, "Ratoon rice mapping based on Sentinel-1 and Sentinel-2 imagery," *Remote Sensing Applications: Society and Environment,* p. 101592, 2025.

[17] V. Tiwari, MG. Tulbure, J. Caineta, MD. Gaines, V. Perin, M. Kamal, TJ. Krupnik and MA. Aziz, "Automated in-season rice crop mapping using Sentinel time-series data and Google Earth Engine: A case study in climate-risk prone Bangladesh," *Journal of Environmental Management,* vol. 351, p. 119615, 2024.

[18] X. Li, C. Sun, H. Meng, X. Ma, G. Huang, and X. Xu, "A novel efficient method for land cover classification in fragmented agricultural landscapes using sentinel satellite imagery," *Remote Sensing,* vol. 14, no. 9, p. 2045, 2022.

[19] P. Wei, H. Ye, S. Qiao, R. Liu, C. Nie, B. Zhang, L. Song and S. Huang, "Early crop mapping based on sentinel-2 time-series data and the random forest algorithm," *Remote Sensing,* vol. 15, no. 13, p. 3212, 2023.

[20] E. Rahimi and C. Jung, "The efficiency of long short-term memory (LSTM) in phenology-based crop classification," *Korean Journal of Remote Sensing,* vol. 40, no. 1, pp. 57-69, 2024.

[21] Y. Xie, L. Xu, H. Zhang, M. Song, J. Ge, and F. Wu, "Tropical Rice Mapping Using Time-Series SAR Images and ESF-Seg Model in Hainan, China, from 2019 to 2023," *Remote Sensing,* vol. 17, no. 2, 2025.

[22] X. Shi, Z. Chen, H. Wang, D.-Y. Yeung, W.-K. Wong, and W.-c. Woo, "Convolutional LSTM network: A machine learning approach for precipitation nowcasting," *Advances in neural information processing systems,* vol. 28, 2015.

[23] L. Liu, X. Xiao, Y. Qin, J. Wang, X. Xu, Y. Hu and Z. Qiao, "Mapping cropping intensity in China using time series Landsat and Sentinel-2 images and Google Earth Engine," *Remote Sensing of Environment,* vol. 239, p. 111624, 2020.

[24] H. Nie, Y. Lin, W. Luo, and G. Liu, "Rice cropping sequence mapping in the tropical monsoon zone via agronomic knowledge graphs integrating phenology and remote sensing," *Ecological Informatics,* vol. 87, p. 103075, 2025.

[25] S. Park, J. Im, S. Park, C. Yoo, H. Han, and J. Rhee, "Classification and mapping of paddy rice by combining Landsat and SAR time series data," *Remote Sensing,* vol. 10, no. 3, p. 447, 2018.

[26] Z. He, S. Li, Y. Wang, L. Dai, and S. Lin, "Monitoring rice phenology based on backscattering characteristics of multi-temporal RADARSAT-2 datasets," *Remote Sensing,* vol. 10, no. 2, p. 340, 2018.

[27] L. Carrasco, A. W. O'Neil, R. D. Morton, and C. S. Rowland, "Evaluating combinations of temporally aggregated Sentinel-1, Sentinel-2 and Landsat 8 for land cover mapping with Google Earth Engine," *Remote Sensing,* vol. 11, no. 3, p. 288, 2019.

[28] F. Namazi, M. Ezoji, and E. G. Parmehr, "Paddy Rice mapping in fragmented lands by improved phenology curve and correlation measurements on Sentinel-2 imagery in Google earth engine," *Environmental Monitoring and Assessment,* vol. 195, no. 10, p. 1220, 2023.

[29] F. Namazi, M. Ezoji, and E. Ghanbari Parmehr, "A Phenology Based Paddy Rice Mapping by Correlation Analysis on Sentinel-1/2 Imagery in Fragmented Lands Using GEE Platform," *Journal of AI and Data Mining,* 2025.

[30] F. Gascon, C. Bouzinac, O. Thépaut, M. Jung, B. Francesconi, J. Louis, V. Lonjou and B. Lafranc, "Copernicus Sentinel-2A calibration and products validation status," *Remote Sensing,* vol. 9, no. 6, p. 584, 2017.

[31] C. J. Tucker, "Red and photographic infrared linear combinations for monitoring vegetation," *Remote sensing of Environment,* vol. 8, no. 2, pp. 127-150, 1979.

[32] X. Xiao, *S. Boles, J. Liu, D. Zhuang and S. Frolking*, "Mapping paddy rice agriculture in southern China using multi-temporal MODIS images," *Remote sensing of environment,* vol. 95, no. 4, pp. 480-492, 2005.

[33] Y. Shao, N. Ma, M. Chen, C. Zhang, and Y. Cui, "Machine Learning in Landscape Architecture: A Comprehensive Review of Advancements, Applications, and Future Directions," *Buildings,* vol. 15, no. 21, p. 3827, 2025.

[34] M. Zhang, H. Lin, G. Wang, H. Sun, and J. Fu, "Mapping paddy rice using a convolutional neural network (CNN) with Landsat 8 datasets in the Dongting Lake Area, China," *Remote Sensing,* vol. 10, no. 11, p. 1840, 2018.

[35] A. Graves and J. Schmidhuber, "Framewise phoneme classification with bidirectional LSTM and other neural network architectures," *Neural networks,* vol. 18, no. 5-6, pp. 602-610, 2005.

[36] M. Marjani, M. Mahdianpari, and F. Mohammadimanesh, "CNN-BiLSTM: A novel deep learning model for near-real-time daily wildfire spread prediction," *Remote Sensing,* vol. 16, no. 8, p. 1467, 2024.

[37] V. Ashish, "Attention is all you need," *Advances in neural information processing systems,* vol. 30, p. I, 2017.

[38] Y.-L. Chang, TH. Tan, TH. Chen, JH. Chuah, L. Chang, MC. Wu, NB. Tatini, SC. Ma and M. Alkhaleefah, "Spatial-temporal neural network for rice field classification from SAR images," *Remote Sensing,* vol. 14, no. 8, p. 1929, 2022.

[39] G. Shen and J. Liao, "Paddy Rice Mapping in Hainan Island Using Time-Series Sentinel-1 SAR Data and Deep Learning," *Remote Sensing,* vol. 17, no. 6, 2025.

[40] X. Guan, C. Huang, G. Liu, X. Meng, and Q. Liu, "Mapping rice cropping systems in Vietnam using an NDVI-based time-series similarity measurement based on DTW distance," *Remote Sensing,* vol. 8, no. 1, p. 19, 2016.

فراتر از شاخص‌های سری زمانی خام: نقشه‌برداری مقاوم شالیزار با چارچوب LSTM مبتنی بر فنولوژی با استفاده از داده‌های ماهواره‌ای چند حسگری

فاطمه نمازی[1]، مهدی ازوجی[1,*] و عبادت قنبری پرمهر[2]

[1] دانشکده مهندسی برق و کامپیوتر، دانشگاه صنعتی نوشیروانی بابل، بابل، ایران.

[2] گروه نقشه‌برداری، دانشکده مهندسی عمران، دانشگاه صنعتی نوشیروانی بابل، بابل، ایران.

ارسال ۲۰۲۶/۰۴/۲۸؛ بازنگری ۲۰۲۶/۰۶/۲۹؛ پذیرش ۲۰۲۶/۰۸/۰۱

چکیده:

نقشه‌برداری دقیق شالیزارهای برنج نقش مهمی در تأمین امنیت غذایی، مدیریت منابع آب و برنامه‌ریزی بلندمدت کشاورزی دارد. در این پژوهش، چارچوبی مبتنی بر شبکه حافظه کوتاه‌مدت بلند (LSTM) و آگاه از فنولوژی ارائه شده است که با تلفیق داده‌های سری زمانی چندمنبعی سنتینل-۱و ۲، امکان شناسایی دقیق و مقاوم شالیزارهای برنج را فراهم می‌کند. تصاویر نوری سنتینل۲ و تصاویر راداری مربوط به سنتینل-۱، ابتدا با حذف پیکسل‌های ابری، ترکیب زمانی در بازه‌های ده‌روزه و درون‌یابی مشاهدات از دست رفته پیش‌پردازش شدند تا برای هر پیکسل، یک سری زمانی کامل و یکنواخت شامل ۱۸ گام زمانی در دوره‌ای ۱۸۰ روزه ایجاد شود. سپس سه شاخص NDVI و LSWI از تصاویر سنتینل-۲ و شاخص CR از تصاویر سنتینل-۱ استخراج شدند که به‌ترتیب بیانگر تغییرات سبزینگی پوشش گیاهی، رطوبت سطح زمین و پوشش گیاهی و تغییرات پس‌پراکنش راداری هستند. به‌منظور وارد کردن دانش پیشین فنولوژیک برنج در فرایند طبقه‌بندی، منحنی‌های فنولوژی مرجع برای این شاخص‌ها تهیه شد. در ادامه، با استفاده از تحلیل همبستگی مبتنی بر پنجره لغزان، سری زمانی هر شاخص در سطح پیکسل با منحنی فنولوژی مرجع متناظر مقایسه شد. حاصل این فرایند، سه توالی شباهت زمانی مبتنی بر همبستگی شامل C_NDVI، C_LSWI و C_CR بود که میزان تطابق رفتار زمانی هر پیکسل با الگوی رشد مشخصه برنج را نشان می‌دهند. در مرحله طبقه‌بندی، سه نوع ورودی شامل شاخص‌های خام سری زمانی، ویژگی‌های مبتنی بر همبستگی و ترکیب این دو، به‌طور جداگانه به مدل LSTM داده شدند و عملکرد آن‌ها ارزیابی شد. نتایج نشان داد که ویژگی‌های مبتنی بر همبستگی بهترین عملکرد را داشته و به دقت کلی ۹۹٫۸۱ درصد، نرخ خطای ۰٫۱۹ درصد و امتیاز F1 برابر با ۰٫۹۹۵۰ دست یافته‌اند. همچنین، در مقایسه با شاخص‌های خام سری زمانی و مجموعه ویژگی‌های ترکیبی، این ویژگی‌ها توانستند شالیزارهای برنج را با دقت بیشتری از کلاس‌های دارای رفتار طیفی مشابه، مانند پهنه‌های آبی و پوشش علف‌های هرز، تفکیک کنند. نتایج نشان می‌دهد که ترکیب ویژگی‌های همبستگی مبتنی بر فنولوژی با قابلیت یادگیری زمانیLSTM، رویکردی مؤثر برای نقشه‌برداری دقیق شالیزارهای برنج در اراضی کشاورزی خرد و پراکنده و مناطق دارای ابرناکی زیاد فراهم می‌کند.

کلمات کلیدی: تخمین سطح زیر کشت برنج، فنولوژی برنج، سنتینل-۱و۲، همبستگی، شبکه حافظه کوتاه‌مدت بلند (LSTM) ، گوگل ارث انجین.